

### Supplementary Figure 1

#### Short-term depression is an intrinsic property of ORN-to-PN synapses.

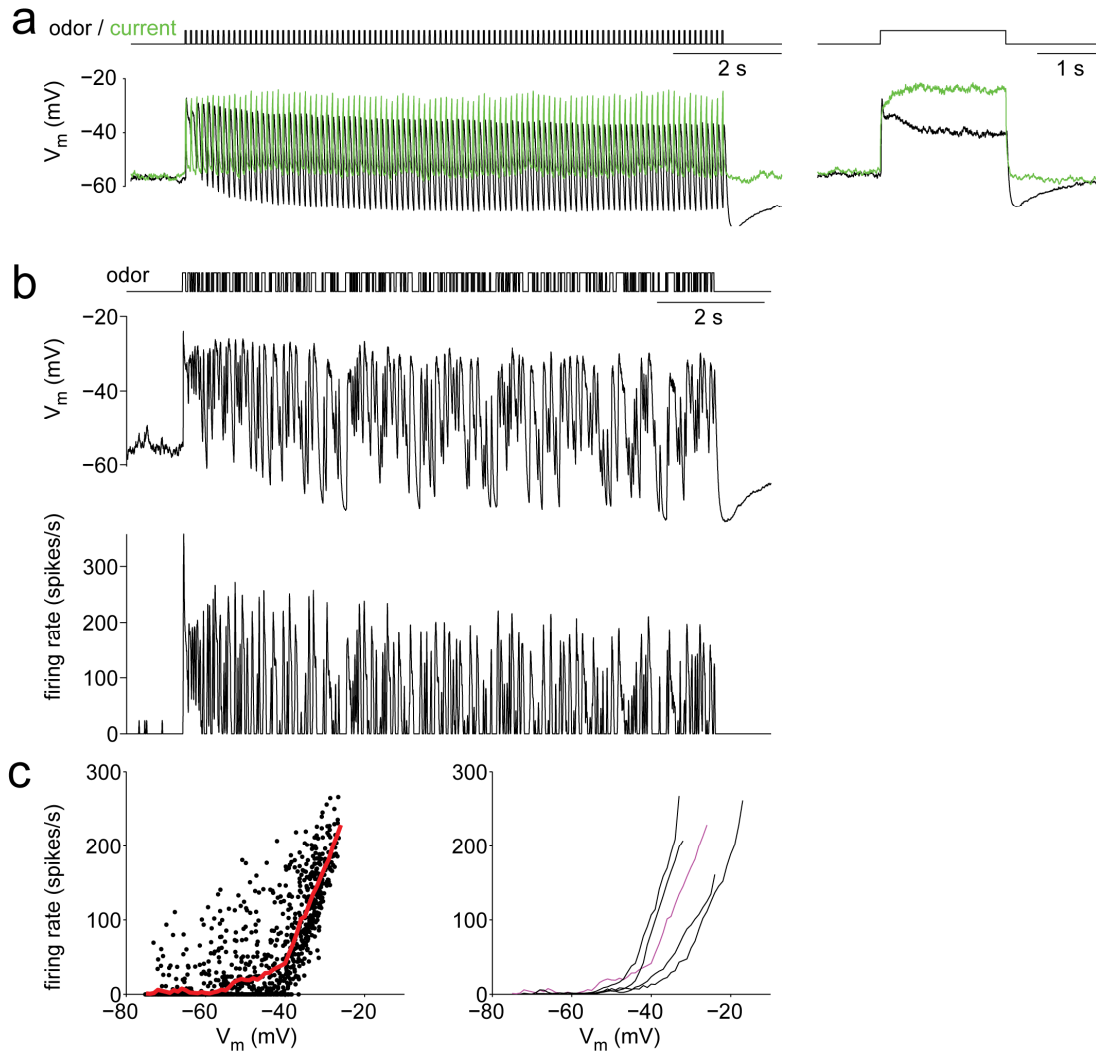
ORN axons in the antennal nerve were stimulated with a train of 20 stimuli at 10 Hz (as in Figure 1b,c). Evoked EPSCs were recorded from PNs in whole-cell voltage clamp mode, both before and after blocking synaptic inhibition (with bath application of 25 – 50  $\mu$ M CGP54626 and 5  $\mu$ M picrotoxin).

a) EPSC amplitudes evoked by each stimulus in a 10 Hz train, normalized to the first EPSC in the train before averaging across PNs, mean  $\pm$  s.e.m.,  $n = 4$  PNs). Blocking inhibition had little effect on the dynamics of short-term depression at this presynaptic firing rate.

b) EPSCs evoked by the entire 10 Hz train (averaged across 4 PNs, 2-5 trials per PN). EPSCs were normalized to the amplitude of the first EPSC prior to averaging.

c) The first EPSC evoked by the train (arrow indicates stimulus time; stimulus artifact is blanked and mended by interpolation).

When inhibition was blocked, some EPSCs were contaminated with currents arising from unclamped spikes in the PN. We excluded experiments where the rate of unclamped spikes was particularly high, but it should be noted that the occurrence of some unclamped spikes makes it difficult to precisely estimate EPSC amplitudes under these conditions.



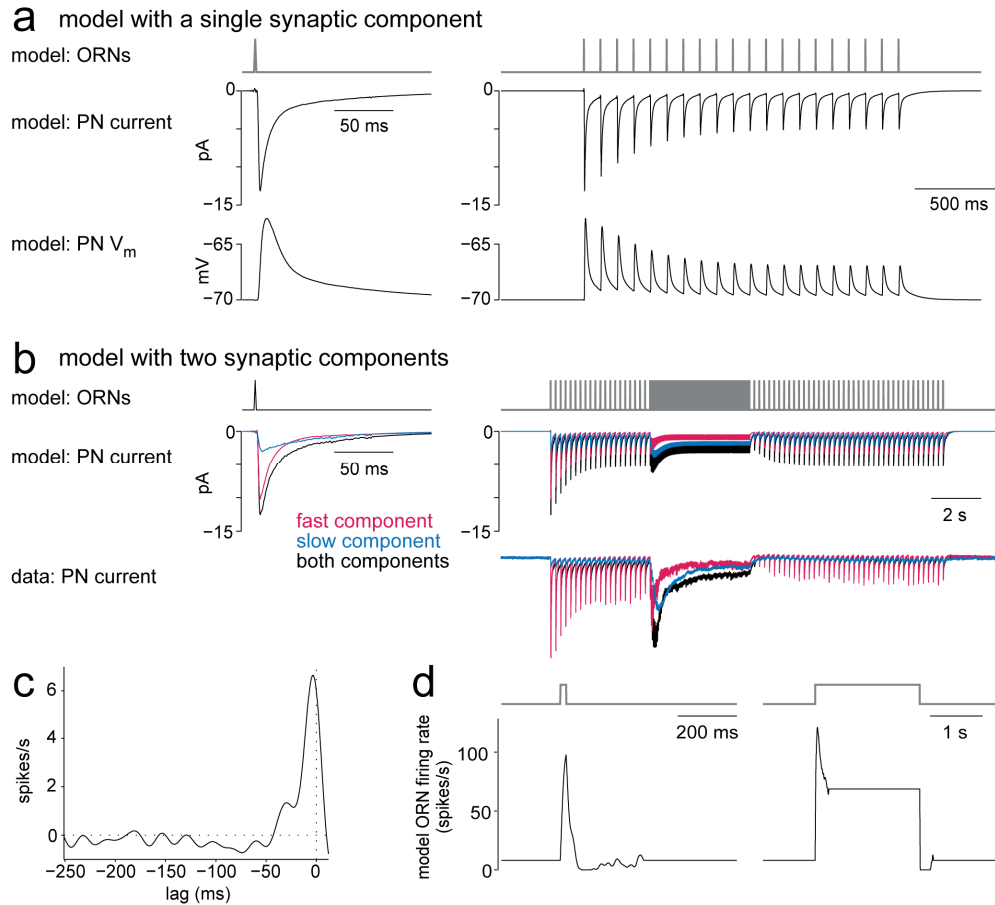
## Supplementary Figure 2

### Intrinsic properties of PNs.

a) When odor pulses are delivered in a dense train, or a long pulse, the PN membrane potential response depresses over time (black traces). Injecting depolarizing current into a PN in the same pattern elicits a membrane potential response that does not depress (green traces). Thus, these PN odor response dynamics do not arise from intrinsic properties of the PN, but rather are due to dynamics in the synaptic input to the PN.

b) The dynamics of PN spiking responses to odors resemble the dynamics of their membrane potential responses. Shown here is a typical example PN, where the odor stimulus was a dense random train of pulses. Both the membrane potential and the firing rate are able to encode even brief pulses, and both can follow a long dense train. As the membrane potential response depresses, the firing rate also depresses. (Note there is a burst of PN spikes at stimulus onset which is not mirrored in the membrane potential; as in many neurons, firing rates in PNs depend to some degree on the rate of change of membrane potential as well as its absolute value. However, a static relationship between membrane potential and spiking captures much of the data, as described below.)

c) Left: in each time bin, PN firing rate is plotted versus membrane potential for one typical recording. Red trace shows average firing rate binned by membrane potential. A static threshold nonlinearity describes much of the data, with a fairly linear relationship above threshold. Right: binned data for 5 typical PNs. These results show that PN firing rates are sensitive to changes in membrane potential over a wide range of membrane potential values. The curve in magenta is the example PN on the left.



### Supplementary Figure 3

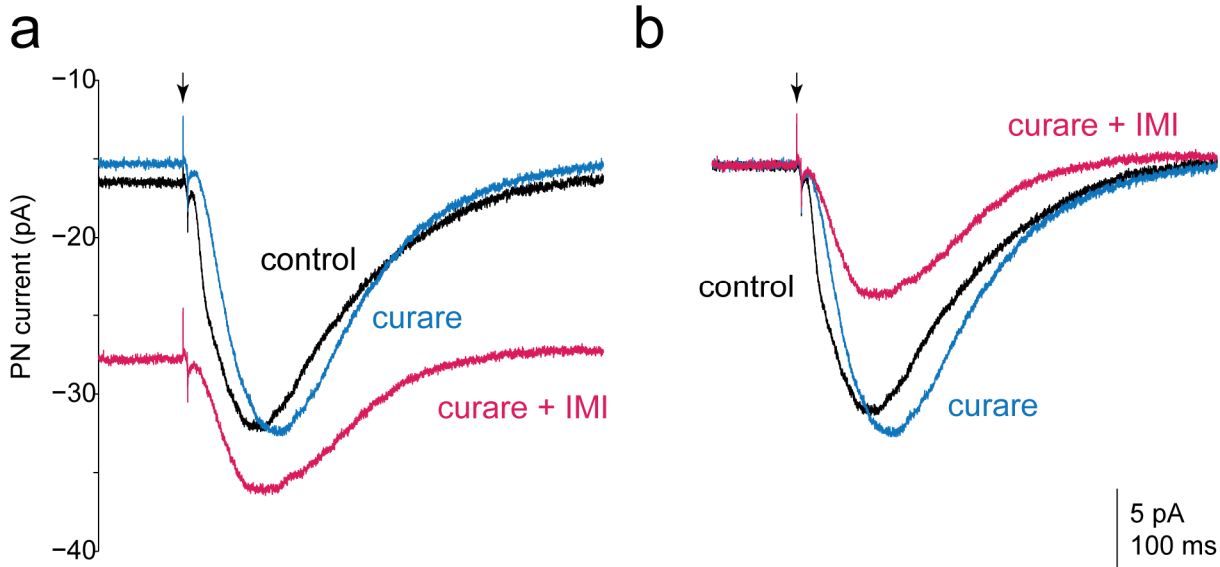
#### Models of PNs and ORNs.

a) Simple synaptic depression model. In this model, synaptic input to a PN depresses with a single set of parameters ( $f$ ,  $\tau$ ), and PN membrane potential is modeled using a passive single compartment model. This illustration shows model current and voltage responses to a single ORN spike (left) and a train of spikes in a single ORN at 10 Hz (right). Parameters of the PN membrane potential model were chosen such that a single spike in one ORN elicited an EPSC with a peak amplitude of about 13.5 pA and an EPSP with a peak depolarization of about 7 mV, consistent with published data (see Methods and ref. 12). Synaptic depression parameters ( $f$ ,  $\tau$ ) were fit to peak EPSC amplitudes in response to 10 Hz antennal nerve stimulation (Figure 1c). The dynamics of simulated responses to 10 Hz spike trains closely resemble our data. This model was used in Figure 1.

b) Model with two postsynaptic components. A two-component model was used in Figure 2g-h, Figure 7, and Figure 8. Here each unitary EPSC was composed of a fast and a slow component. The amplitude of the unitary fast and slow conductances were chosen such that the combined EPSC had an amplitude of about 13.5 pA (in agreement with published data). The relative magnitudes of the two conductances were determined by fitting a biexponential decay to the normalized first EPSC in control conditions. Depression parameters ( $f$ ,  $\tau$ ) for the fast component were fit to EPSCs in IMI. Depression parameters for the slow component were either fit to EPSCs in curare (shown here, Figure 2g-h) or else fit to PN odor responses with inhibition blocked (Figure 7 and Figure 8).

c) ORN filter. To model ORN spike rates in Figure 8, we convolved the binary stimulus waveform with the filter shown here. The filter was extracted by cross-correlating ORN spikes with simultaneously-recorded measurements of odor concentration using a fast photoionization detector, followed by decorrelation by the power spectrum of the odor concentration fluctuations (ref. 64). ORN spikes were recorded from ORNs presynaptic to glomerulus VM7.

d) Model ORN responses to short and long odor pulses. Firing rates were obtained by convolving the ORN filter with the stimulus waveform. All stimuli have an amplitude of 1.



**Supplementary Figure 4**

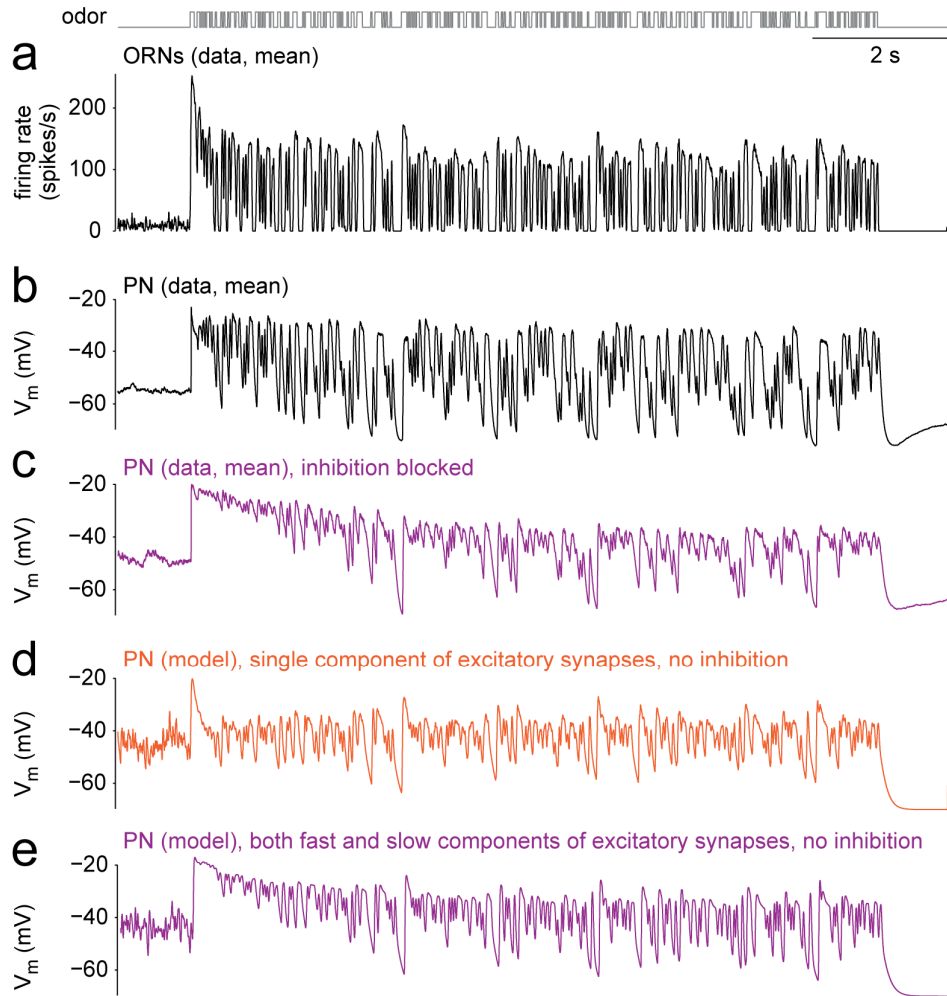
**Pharmacology of acetylcholine-evoked currents.**

a) Mean acetylcholine-evoked currents recorded in voltage-clamp recordings from PNs (glomerulus VM2, DM6, or VM7,  $n=5$  PNs, average of 5-6 trials per PN). Acetylcholine was iontophored into the neuropil for 5 ms at the time indicated (arrows). Bath application of curare ( $10 \mu\text{M}$ ) slows the acetylcholine-evoked current. Adding IMI ( $100 \text{ nM}$ ) together with curare blocks a substantial fraction of the evoked current. Note that IMI ( $100 \text{ nM}$ ) increases the basal holding current, consistent with reports that it can act as a partial agonist (ref. 30).

b) Same as panel a, but with baselines aligned to better illustrate changes in the timecourse of the evoked current.

We note that the two drugs did not completely block the response to iontophoresis of acetylcholine, likely because some of the current evoked by iontophoresis is due to metabotropic receptors. The two drugs together blocked  $94.1 \pm 2.7\%$  of the response to iontophoresis of nicotine ( $10 \text{ ms}$  stimulus duration,  $n=4$ ). In the presence of atropine ( $10 \mu\text{M}$ ), the two drugs blocked  $81\%$  of the response to iontophoresis of acetylcholine ( $n=1$ ). Metabotropic receptor antagonists (atropine at  $10 \mu\text{M}$  and scopolamine at  $10 \mu\text{M}$ ) had no effect on responses to nerve stimulation. Together, these results imply that curare and IMI act on nicotinic acetylcholine receptors, and that most of the current evoked by nerve stimulation is nicotinic. Metabotropic receptors are evidently present on PNs and are activated by iontophoresis of acetylcholine but not by our nerve stimulation protocol.

Acetylcholine chloride was prepared as a  $1 \text{ M}$  solution in water, nicotine hydrogen tartrate as a  $0.25\text{-}1 \text{ M}$  solution in water, atropine as a  $5 \text{ mM}$  stock in water, and scopolamine as a  $1 \text{ mM}$  stock in water. All drugs were obtained from Sigma and stored at  $-4^\circ\text{C}$  as aqueous stocks. Iontophoretic ejection currents were  $+350\text{-}800 \text{ nA}$ , and the constant holding current was  $-10 \text{ nA}$ ; these stimuli were delivered with a constant current generator (World Precision Instruments, Model 260).



**Supplementary Figure 5**

**The slow decay in the odor responses of disinhibited PNs is primarily due to synaptic dynamics, with a minor contribution from ORN firing rate dynamics.**

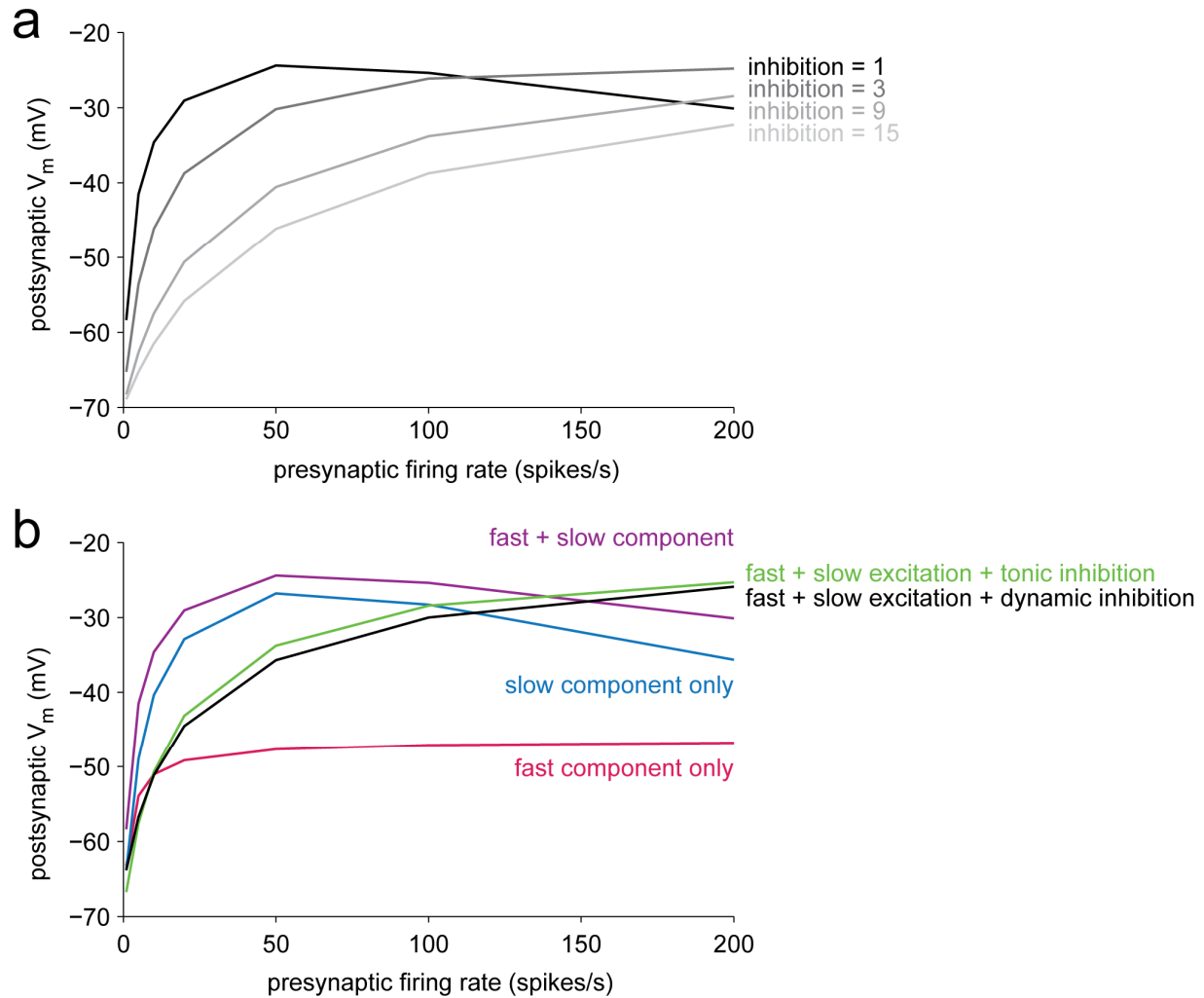
a) ORN firing rates evoked by a dense randomly fluctuating stimulus (valve open 50% of the time). Data represent the average of several recordings from VM7 ORNs. These ORN firing rates decay slowly over time.

b) Mean PN membrane potential responses to the same odor stimuli ( $n=7$  PNs in glomerulus VM7). This is a subset of the data shown in Figure 1g, focusing here on VM7 PNs only.

c) Mean responses of the same cells following blockade of inhibition. This should represent the purely feedforward response of the PN. Note that when ORN responses have reached steady-state, PN responses are still slowly decaying. Thus, much of the slow decay in PN responses cannot be inherited from ORN firing rates, and likely arises from the dynamics of ORN-to-PN synapses. This slow decay is normally masked by inhibition.

d) Output of the single component model without inhibition (same as in Figure 1). Note the slow decay in ORN firing rates is not transmitted to the PNs, because at high presynaptic firing rates, PNs are relatively insensitive to small changes in presynaptic rate. Instead, PN response dynamics are dominated by the dynamics of synaptic transmission.

e) Output of a two-component model without inhibition (acting on the ORN spike rates shown in panel a). Parameters of the fast component were the same as in Figure 2 (fit to EPSCs in IMI). Parameters of the slow component were adjusted to maximize the fit between model output and the disinhibited PN membrane potential shown in panel c. This model captures the slow decay in PN odor responses when inhibition is blocked. This model was used in Figures 7 and 8.

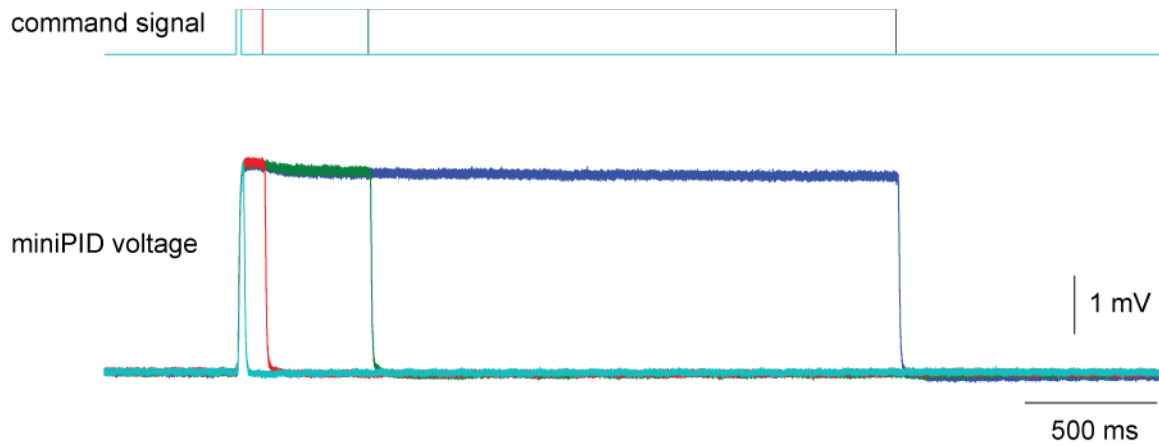


### Supplementary Figure 6

#### Quasi-steady-state responses of our models.

a) Responses of model PNs after 2 s of stimulation, with and without tonic presynaptic inhibition. In this model, ORN-to-PN synapses have both fast and slow components. (This model is equivalent to the one shown in Figure 8, but with tonic inhibition fixed at the pre-odor level, instead of dynamic inhibition.) Here, simulated stimuli were 2-s steps of steady ORN firing rates from zero to a range of levels (1-200 spikes/s). The time-averaged PN membrane potential was measured over the window from 1 s to 2 s after the onset of the stimulus, and was plotted as a function of presynaptic firing rate. As shown in previous theoretical studies (refs. 7,8) the postsynaptic response saturates rapidly as a function of presynaptic firing rate, and adding increasing amounts of tonic presynaptic inhibition causes the postsynaptic response to saturate at a higher presynaptic firing rate. Small amounts of presynaptic inhibition have a more profound effect on the response to low presynaptic firing rates than on the response to high presynaptic firing rates.

b) Model responses after 2 s of stimulation (calculated as in panel a), as a function of presynaptic firing rate for the different model components. The fast component of excitation at ORN-to-PN synapses has a relatively small dynamic range for encoding tonic changes in presynaptic firing rate, while the slow component shows a larger dynamic range. A model with both fast and slow components shows a larger dynamic range but saturates at a low presynaptic firing rate. Both tonic and dynamic inhibition cause the postsynaptic response to saturate more gradually as a function of presynaptic firing rate. Here dynamic inhibition was modeled as in Figure 8, and tonic inhibition was fixed at the pre-odor level of inhibition in the dynamic model.



### Supplementary Figure 7

#### Testing the speed and stability of the odor delivery device.

In this test, the valve that delivers odor to the preparation was opened for 20 ms, 100 ms, 500 ms, or 2.5 s. Traces at top show these command signals. The odor was 2-hepanone, here used at 1:10 in order to increase the signal-to-noise ratio of detector measurements. A photoionization detector (miniPID 200B, Aurora Scientific) was placed at the position of the preparation in order to measure the time course of the odor concentration change at the preparation. These measurements showed that the odor delivery device could reliably deliver square pulses over a wide range of durations, and that the concentration of the odor at the fly's location was reasonably stable.